

## Physics-Informed Neural Networks for Quantum Control

Ariel Norambuena<sup>1,\*</sup>, Marios Mattheakis<sup>2</sup>, Francisco J. González<sup>3</sup>, and Raúl Coto<sup>3,4,†</sup>

<sup>1</sup>*Centro de Optica e Información Cuántica, Universidad Mayor, Camino la Piramide 5750, Huechuraba, Santiago, Chile*

<sup>2</sup>*John A. Paulson School of Engineering and Applied Sciences, Harvard University, Cambridge, Massachusetts 02138, USA*

<sup>3</sup>*Centro de Investigación DAiTA Lab, Facultad de Estudios Interdisciplinarios, Universidad Mayor, Santiago 7560908, Chile*

<sup>4</sup>*Department of Physics, Florida International University, Miami, Florida 33199, USA*

 (Received 27 June 2022; revised 14 October 2022; accepted 6 December 2023; published 3 January 2024)

Quantum control is a ubiquitous research field that has enabled physicists to delve into the dynamics and features of quantum systems, delivering powerful applications for various atomic, optical, mechanical, and solid-state systems. In recent years, traditional control techniques based on optimization processes have been translated into efficient artificial intelligence algorithms. Here, we introduce a computational method for optimal quantum control problems via physics-informed neural networks (PINNs). We apply our methodology to open quantum systems by efficiently solving the state-to-state transfer problem with high probabilities, short-time evolution, and using low-energy consumption controls. Furthermore, we illustrate the flexibility of PINNs to solve the same problem under changes in physical parameters and initial conditions, showing advantages in comparison with standard control techniques.

DOI: [10.1103/PhysRevLett.132.010801](https://doi.org/10.1103/PhysRevLett.132.010801)

Optimal quantum control (QC) is crucial to exploit all the advantages of quantum systems, ranging from entangled states preparation and quantum registers to quantum sensing. Nowadays, QC can be achieved by means of controllable dissipative dynamics [1,2], measurement-induced backaction [3–5], Lyapunov control [6,7], optimal pulse sequences [8], and differentiable programming [9,10]. These QC techniques serve multiple purposes including state preservation, state-to-state transfer [11], dynamical decoupling in open systems [12–14], and trajectory tracking [15,16]. Furthermore, we have witnessed powerful applications across multiple platforms, including atomic systems [17,18], light-matter systems [19,20], solid-state devices [21,22], trapped ions [23], and others. Dynamical QC stems from a time-dependent Hamiltonian that steers the dynamics [24], and it is subjected to several constraints like laser power, inhomogeneous frequency broadening, and relaxation processes, to name a few. Therefore, finding the optimal sequence for QC is highly cumbersome and generally depends on the system.

Complex computational calculations are at the forefront of numerical methods to tackle simulation of quantum systems. For instance, a parametrization of quantum states in terms of neural networks has enabled the approximation of many-body wave functions in closed quantum systems [25–27], and it has also been extended to approach the density operator in open dynamics (dissipative) [28–33]. Along these ideas, other models have focused on hybrid implementations [34–36], probabilistic formulations based on positive operator-valued measure [37,38], or data-driven model via time-averaged generators [39]. Overall,

estimating the dynamics of open quantum systems is a challenging problem. Here, machine learning provides versatile and promising algorithms to expand our alternatives toward completing this task [40–46]. However, combining time evolution and QC with artificial intelligence, being solved within a single deep learning method still needs to be explored.

Neural networks (NNs) are commonly trained with data allowing them to learn the dynamics of quantum systems. However, NNs that preserve the underlying physical laws without preliminary data would have practical advantages. Hence, physics-informed neural networks (PINNs) have been introduced as a new artificial intelligence paradigm that requires only the model itself [47,48]. This is a general physics-informed machine learning framework that has been applied to solve high-dimensional partial differential equations [49,50], many-body quantum systems [51,52] and quantum fields [53], inverse problems using sparse and noisy data [54], and to discover underlying physics hidden in data structures [55,56]. Since PINNs are coded using physical laws, they can be applied to any quantum evolution where the model is well known [57–63].

In this Letter, we introduce a novel PINN architecture to find optimal control functions in open quantum systems. This is a data-free inverse modeling deep learning approach with a target dynamical behavior instead of data. Our approach suggests smooth control functions for driving quantum states to a preselected target state.

Let us consider the following  $n$ -dimensional nonautonomous dynamical system:

$$\dot{\mathbf{x}} = A(\boldsymbol{\lambda}, \mathbf{u}(t))\mathbf{x}(t), \quad \mathbf{x}(0) = \mathbf{x}_0, \quad \mathbf{u}(0) = \mathbf{u}_0, \quad (1)$$

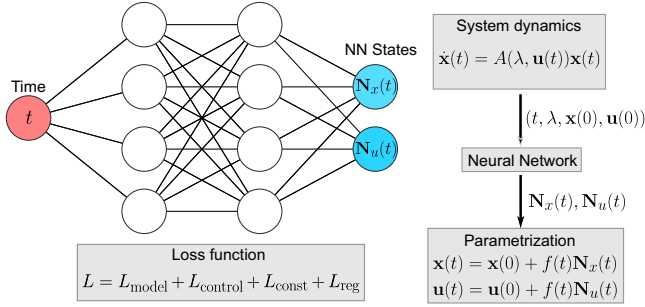


FIG. 1. PINNs architecture for solving quantum control problems. Quantum evolution can be translated into a dynamical system  $\dot{\mathbf{x}}(t) = A(\boldsymbol{\lambda}, \mathbf{u}(t))\mathbf{x}(t)$ , where  $\mathbf{x}(t)$  and  $\mathbf{u}(t)$  are the state and control vectors, respectively, and  $\boldsymbol{\lambda}$  are the system parameters. The input data (red circle) is given by the discrete time vector  $t$ , and the outputs of the neural network (NN) are  $\mathbf{N}_x(t)$  and  $\mathbf{N}_u(t)$  (blue circle). By minimizing the loss function  $L$  the NN discover  $\mathbf{N}_{x,u}(t)$  for the parametrized solutions  $\mathbf{x}(t)$  and  $\mathbf{u}(t)$ .

where  $\mathbf{x}(t) = (x_1, \dots, x_n)^T \in \mathbb{R}^n$ ,  $\mathbf{u}(t) = (u_1, \dots, u_m)^T \in \mathbb{R}^m$ , and  $\boldsymbol{\lambda} = (\lambda_1, \dots, \lambda_s)^T \in \mathbb{R}^s$  are the state, control, and parameter vectors (with  $n, m, s \geq 1$  and  $m \leq n^2$ ), respectively. Here,  $A(\boldsymbol{\lambda}, \mathbf{u}(t))$  is a real  $n \times n$  dynamical matrix that depends on  $\mathbf{u}(t)$  (control) and  $\boldsymbol{\lambda}$  (parameters).

Given  $\boldsymbol{\lambda}$  and  $\mathbf{x}(t)$  satisfying Eq. (1), we can apply machine learning to discover an optimal control vector  $\mathbf{u}(t)$  such that the system evolves from  $\mathbf{x}(0)$  to some desired target state  $\mathbf{x}_d$ . Techniques based on optimal control [64], Lyapunov control theory [6], or linear control theory are based on optimization rules to find a suitable control vector  $\mathbf{u}(t)$ . Therefore, the main idea is to construct a PINN that minimizes a loss function to achieve optimal quantum control.

A feed forward NN is a powerful universal approximator for any vector function  $F: \mathbb{R}^p \mapsto \mathbb{R}^q$  ( $r, q \geq 1$ ) (universal approximation theorem) [65]. Let us consider the NN architecture illustrated in Fig. 1 as a new paradigm to solve quantum control problems. We use an equally distributed time array  $t = (t_1, \dots, t_M)$  as the input to the NN, with  $M$  representing the dimension of the sample points. PINNs do not require a structured mesh; thus,  $t_i$  can be arbitrarily discretized. The NN consists of multiple hidden layers with activation function  $\sin(\cdot)$  for the hidden neurons. This choice of activation has been shown to improve PINNs' performance in solving nonlinear dynamical systems [66] and high-dimensional partial differential equations [50]. The outputs of the NN are the solutions  $\mathbf{N}_x(t) \in \mathbb{R}^n$  and  $\mathbf{N}_u(t) \in \mathbb{R}^m$ . We construct a neural state and control vectors that identically satisfy the initial conditions by using a hard constraint,  $\mathbf{x}(t) = \mathbf{x}(0) + f(t)\mathbf{N}_x(t)$  and  $\mathbf{u}(t) = \mathbf{u}(0) + f(t)\mathbf{N}_u(t)$ , where  $f(t) = 1 - e^{-t}$  is a function satisfying  $f(0) = 0$  [66]. This hard constraint approach avoids numerical errors in the initial conditions. The network parameters, weights and biases, are randomly initialized, and then they are optimized by minimizing a

physics-informed loss function defined by

$$L = L_{\text{model}} + L_{\text{control}} + L_{\text{const}} + L_{\text{reg}}. \quad (2)$$

The component  $L_{\text{model}}$  describes the system dynamics:

$$L_{\text{model}} = \sum_{i=1}^M \|\dot{\mathbf{x}}(t_i) - A(\boldsymbol{\lambda}, \mathbf{u}(t_i))\mathbf{x}(t_i)\|^2, \quad (3)$$

with  $\|\cdot\|$  representing a Euclidean distance. The time derivatives in the neural solutions are computed using the automatic differentiation method provided by PyTorch package [67]. By minimizing the above functional, the state vector will approximately satisfy the system dynamics and, thus, the underlying physics. The second term on the right-hand side of Eq. (2) represents the control, that reads

$$L_{\text{control}} = \eta \sum_{i=1}^M \|\mathbf{x}(t_i) - \mathbf{x}_d\|^2, \quad 0 \leq \eta \leq 1, \quad (4)$$

where the factor  $\eta$  regulates the relevance of the control condition compared to the leading model component  $L_{\text{model}}$ . Note that  $\mathbf{x}_d$  could be a constant (regulation) or time-dependent (trajectory tracking) vector depending on the control scheme. The term  $L_{\text{const}}$  could take into account additional physical constraints for the state or control vector, respectively, such as probability conservation or holonomic constraints of the form  $H(\mathbf{x}, \mathbf{u}, t) = 0$ . Finally,  $L_{\text{reg}}$  is a standard regularization loss term that encourages the network parameters to take relatively small values avoiding overfitting. We remark that imposing initial conditions into the loss function (soft constraint) is also possible, as illustrated in Ref. [47]. The comparison between soft and hard constraints is discussed in Ref. [68]. The effect of overfitting will be the prediction of a too complex  $\mathbf{u}(t)$ , which might be practically unfeasible for designing a real control. We introduce  $L_{\text{reg}}$  as an  $l_2$ -norm of the network weights  $L_{\text{reg}} = \chi \sum_i w_i^2$ , where  $\chi$  is the regularization parameter.

The minimization of the loss function given in Eq. (2) yields NN predictions that obey the underlying physics and suggest optimal control functions. For the training [minimization of Eq. (2)], we employ Adam optimizer [76]. Moreover, the points  $t_i$  are randomly perturbed during the training iteration—this method has been shown to improve the training and the neural predictions [49,66]. To highlight the method and keep the presentation elegant, we focused on low-dimensional Hilbert space examples. In the Supplemental Material, we demonstrate that the proposed PINN can successfully deal with larger systems [68].

We consider a two-level system as a proof-of-principle example to illustrate the use of PINNs for QC. We address the problem of generating Gibbs (mixed) states of the form  $\rho_{\text{Gibbs}} = Z^{-1} \sum_j e^{-\beta E_j} |j\rangle\langle j|$ , with  $Z = \text{Tr}(e^{-\beta H})$  (partition function) and  $\beta = (k_B T)^{-1}$  (inverse temperature). The preparation of mixed states is relevant for simulating high-temperature superconductivity in variational quantum

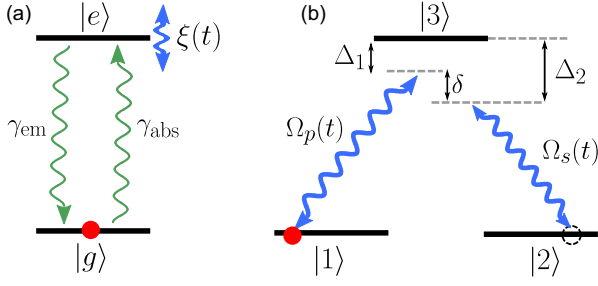


FIG. 2. (a) Open two-level system controlled by a time-dependent modulation  $\xi(t)$ . Losses are included through absorption ( $\gamma_{\text{abs}}$ ) and emission ( $\gamma_{\text{em}}$ ) processes. (b) Three-level  $\Lambda$  system controlled by two driving fields  $\Omega_p(t)$  and  $\Omega_s(t)$ . We include pure dephasing rates  $\gamma_i$  ( $i = 1, 2, 3$ ) acting on each state  $|i\rangle$ . One- ( $\Delta_{1,2}$ ) and two-photon ( $\delta$ ) detunings are considered in our simulations.

circuits [77]. In addition, QC of two-level systems is also relevant in the context of pulse reverse engineering [78], feedback control [3], optimal control theory [64], and controllable quantum dissipative dynamics [79]. Quantum transitions can be written in terms of the operators  $\sigma_{ij} = |i\rangle\langle j|$  ( $i, j = e, g$ ), with  $|e\rangle$  ( $|g\rangle$ ) the excited (ground) state. Let us consider the following Hamiltonian with a phase damping control,

$$H(t) = \omega_z \sigma_z + \omega_x \sigma_x + \xi(t) \sigma_{ee}, \quad (5)$$

with  $\omega_{x,z}$  representing system parameters and  $\xi(t)$  describing the unknown control field. Here,  $\sigma_z = \sigma_{ee} - \sigma_{gg}$  and  $\sigma_x = \sigma_{eg} + \sigma_{ge}$ . Here,  $\xi(t)$  is the control used to generate Gibbs states. To train our PINN we use the Markovian master equation,  $\dot{\rho} = -i[H(t), \rho] + \sum_{i=1,2} \gamma_i [L_i \rho L_i^\dagger - (1/2)\{L_i^\dagger L_i, \rho\}]$ , with  $[\cdot, \cdot]$  ( $\{\cdot, \cdot\}$ ) representing the commutator (anticommutator). The amplitude damping channel is described by absorption ( $L_1 = \sigma_{eg}$ ) and emission ( $L_2 = \sigma_{ge}$ ) processes with rates  $\gamma_1 = \gamma_{\text{abs}}$  and  $\gamma_2 = \gamma_{\text{em}}$ , respectively; see Fig. 2(a). In what follows, we use  $\omega_z = 2$ ,  $\omega_x = 1$ ,  $\gamma_{\text{abs}} = 0.1$ ,  $\gamma_{\text{em}} = 0.3$ , and  $\xi(0) = 0$ . For  $\xi(t) = 0$ , we get the steady state (SS)  $\rho^{\text{SS}} = 0.2775|e\rangle\langle e| + 0.7225|g\rangle\langle g| + [(-0.1106 + i0.0083)|g\rangle\langle e| + \text{c.c.}]$ . Thus, we use  $\xi(t)$  to drive the system to another SS, say,  $\rho_d = (1/2)(|e\rangle\langle e| + |g\rangle\langle g|)$ . Hence, we introduce the real state vector  $\mathbf{x}(t) = (x_1, x_2, x_3, x_4)^T = [\rho_{gg}, \rho_{ee}, \text{Re}(\rho_{eg}), \text{Im}(\rho_{eg})]^T$ , where  $\rho_{ij} = \langle i|\rho(t)|j\rangle$  are the elements of the density matrix. The dynamics can be written as  $\dot{\mathbf{x}} = A(\lambda, \mathbf{u}(t))\mathbf{x}(t)$ , with

$$A(\lambda, \mathbf{u}(t)) = \begin{pmatrix} -\gamma_{\text{abs}} & \gamma_{\text{em}} & 0 & -2\omega_x \\ \gamma_{\text{abs}} & -\gamma_{\text{em}} & 0 & 2\omega_x \\ 0 & 0 & -\Gamma & -2\omega_z - \xi(t) \\ \omega_x & -\omega_x & 2\omega_z + \xi(t) & -\Gamma \end{pmatrix}, \quad (6)$$

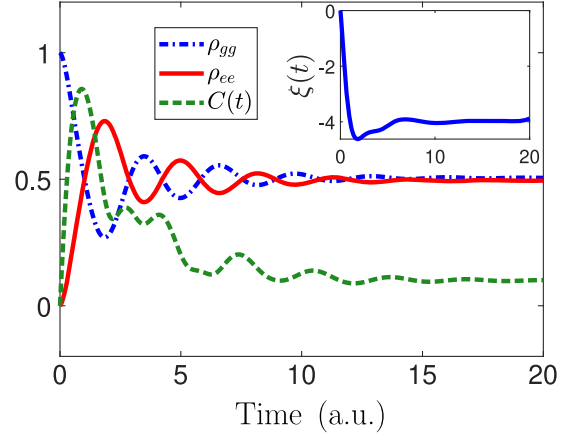


FIG. 3. Evolution of populations  $\rho_{gg}(t)$ ,  $\rho_{ee}(t)$ , and coherence  $C(t)$  using the control function  $\xi(t)$  predicted by the PINN. The architecture of the NN consists of 4 hidden layers of 200 neurons, it is trained for  $4 \times 10^4$  epochs with a learning rate  $10^{-4}$ ,  $\chi = 10^{-3}$ , and  $\eta = 1$ . The inset figure shows the PINN solution for the control function.

where  $\lambda = (w_x, w_z, \gamma_{\text{abs}}, \gamma_{\text{em}})$  is the set of parameters,  $\mathbf{u}(t) = \xi(t)$  is the control vector that needs to be discovered, and  $\Gamma = (1/2)(\gamma_1 + \gamma_2)$  is the effective dephasing rate. We remark that all results concerning the time evolution are simulated from a traditional ordinary differential equation (ODE) solver using the control obtained from the PINN. In Fig. 3, we plot the dynamics using the PINN's prediction for the control  $\xi(t)$  (inset). The PINN discovers an optimal Gibbs state preservation with fidelity  $F(\rho(t), \rho_d) = (\text{Tr}[\rho^{1/2}(t)\rho_d\rho^{1/2}(t)]^{1/2})^2 = 0.99$  (for  $t \geq 20$ ), and the steady state approaches to  $\rho_d$  within an error of 1% for each component of the density matrix [68]. We remark that our result outperforms the analytically optimized solution that finds  $\rho_{gg}^{\text{SS}} = 0.549$ ,  $\rho_{ee}^{\text{SS}} = 0.4510$ ,  $\text{Re}(\rho_{eg}) = 0$ , and  $\text{Im}(\rho_{eg}) = 0.049$ , for a constant control  $\xi^{\text{SS}} = -4$  (see Ref. [68] for further details). The latter explains the asymptotic behavior for  $\xi(t)$  predicted by the PINN. Moreover, we note in Fig. 3 that the quantum coherence  $C(t) = 2|\rho_{eg}(t)|$  is highly activated during the transient dynamics in order to generate an equally distributed mixed state, but it asymptotically reaches  $C \approx 0.1014$ .

We now focus on a  $\Lambda$  configuration with two control fields [see Fig. 2(b)], a platform for studying electromagnetically induced transparency [80,81], coherent population trapping [82,83], and adiabatic population transfer [84]. The latter has been dubbed stimulated Raman adiabatic passage (STIRAP) [85]. Let us begin with the system Hamiltonian  $H = \sum_i E_i \sigma_{ii} + H_c(t)$ , where  $E_i$  stands for the eigenenergies,  $\sigma_{ij} = |i\rangle\langle j|$ , and  $H_c(t)$  is the control Hamiltonian. In a multirotating frame and after the rotating wave approximation, the dynamics of the three-level system is governed by ( $\hbar = 1$ )

$$H(t) = \delta\sigma_{22} + \Delta_1\sigma_{33} + \left(\frac{\Omega_p(t)}{2}\sigma_{31} + \frac{\Omega_s(t)}{2}\sigma_{32} + \text{H.c.}\right), \quad (7)$$

where  $\Delta_1 = E_3 - E_1 - \omega_p$  and  $\Delta_2 = E_3 - E_2 - \omega_s$  are the one-photon detunings that originate from off-resonant driving fields with frequencies  $\omega_p$  and  $\omega_s$ , while  $\delta = \Delta_1 - \Delta_2$  is the two-photon detuning. Here,  $\Omega_p(t)$  and  $\Omega_s(t)$  are the control fields to be found. A similar Hamiltonian can be obtained from the interaction of a nitrogen-vacancy center with a carbon-13 nuclear spin [86,87]. We aim to find the optimal control pulses  $[\Omega_p(t)$  and  $\Omega_s(t)]$  to transfer population from state  $|1\rangle$  to state  $|2\rangle$  via the lossy intermediary state  $|3\rangle$ . Our goal is to train a PINN that completes the task reaching high fidelity, with (i) minimizing the population in the state  $|3\rangle$  and (ii) minimizing the pulse area. We train our model using the Markovian master equation ( $\hbar = 1$ ),

$$\dot{\rho} = -i[H(t), \rho] + \sum_{i=1}^3 \gamma_i (2\sigma_{ii}\rho\sigma_{ii} - \sigma_{ii}\rho - \rho\sigma_{ii}), \quad (8)$$

where  $\gamma_i > 0$  are dephasing rates. We set  $\gamma_3 = 0.14$  and  $\gamma_1 = \gamma_2 = 10^{-3}$  to account for larger dissipation in the excited state. We use the real vector  $\mathbf{z} = (\rho_{11}, \rho_{22}, \rho_{33}, \text{Re}[\rho_{12}], \text{Im}[\rho_{12}], \text{Re}[\rho_{13}], \text{Im}[\rho_{13}], \text{Re}[\rho_{23}], \text{Im}[\rho_{23}])^T$  to write the dynamics (details are given in Ref. [68]).

In Fig. 4(a), we show the population evolution and the predicted NN solutions for the control fields  $\Omega_{s,p}(t)$ . Note

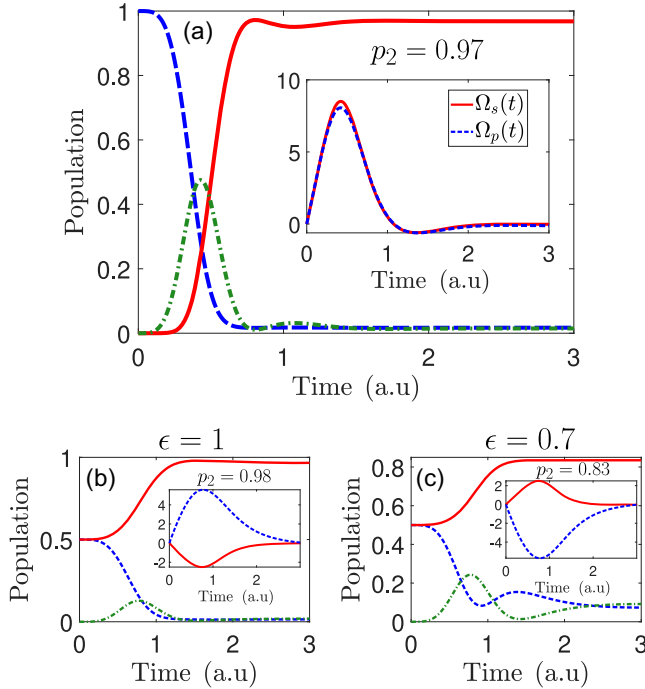


FIG. 4. (a) Population dynamics for the  $\Lambda$  system using  $\Omega_{s,p}(t)$  predicted by the PINN. The PINN allows us to polarize the system starting from a (b) coherent ( $\epsilon = 1$ ) and (c) quasithermal state ( $\epsilon = 0.7$ ). The architecture of the NN includes 5 hidden layers of 150 neurons and it is optimized over  $2 \times 10^4$  training epochs with learning rate  $8 \times 10^{-3}$ ,  $\eta = 0.2$ , and  $\chi = 2.8 \times 10^{-3}$  [68]. The inset figures show the PINN solution for the pulses  $\Omega_{s,p}(t)$  considering different initial conditions.

that our PINN successfully delivers a population transfer with smooth pulses. Furthermore, it attempts to implement a counterintuitive sequence, turning on the Stokes pulse  $\Omega_s$  (red solid line) at the same time that the pump field  $\Omega_p$  (blue dashed line)—for a genuine counterintuitive sequence like STIRAP, Stokes pulse precedes the pump pulse. This is remarkable, considering that the PINN does not know QC theory or the relevance of following a dark state evolution. It is worth noting that the Stokes pulse shown in the inset of Fig. 4(a) triggers the  $|2\rangle \leftrightarrow |3\rangle$  transition, which in STIRAP serves the purpose of preparing a dark state [87], since initially all the population is in state  $|1\rangle$ .

For completeness, we consider a more challenging initial state given by  $\rho(0) = \sigma_{11}/2 + \sigma_{22}/2 + \epsilon(\sigma_{12} + \sigma_{21})/2$ . For  $\epsilon = 0$ , we end up with a fully mixed state (without quantum coherence), while  $\epsilon = 1$  provides a balanced coherent state. Our PINN can handle this new task without changing the network's architecture, showing that PINNs provide a general and adaptive framework for inverse design (standard methods are not designed for this task). In Figs. 4(b) and 4(c), we show the population transfer and the corresponding pulse sequences for  $\epsilon = 1$  and  $\epsilon = 0.7$ , respectively. Note that the PINN updates the pulses to deliver good polarizations.

For a thorough benchmarking, we consider other control methods besides STIRAP [84,85], such as stimulated Raman exact passage (STIREP) [88], inverse engineering (Inv. Eng.) [89,90] and modified superadiabatic transitionless driving (MODSATD) [21,91]. For detailed calculations of these pulses, see [68]. In Table I we show a comparison. One can observe that PINN itself speeds up the population transfer with a high fidelity and using a small amount of energy. The transfer time  $t_f$  is defined as the time required to reach the highest probability in the target state (more details in Ref. [68]). The predicted control functions have the smallest area  $\mathcal{A}$  compared to the other methods. We remark that the regularization  $L_{\text{reg}}$  penalizes the fields for being too large and provides smooth functions. Thus, we can control the amplitudes of the fields and the pulse area to achieve a less power-consuming transfer. Another important advantage of our protocol is the robustness against changes over initial training parameters. It is known that

TABLE I. The population  $p_2 = \text{Tr}[\rho\sigma_{22}]$ , pulse area  $\mathcal{A} = \int_0^{t_f} dt \sqrt{|\Omega_p(t)|^2 + |\Omega_s(t)|^2}$ , and transfer time  $t_f$  (in arbitrary units). In parentheses, we report the values with  $\Delta_1/2\pi = 0.2$  and  $\delta/2\pi = 0.2$ , the one- and two-photon detuning, respectively.

	PINN	STIRAP	STIREP	Inv. Eng.	MODSATD
$p_2$	0.97 (0.93)	0.98 (0.88)	0.98 (0.91)	0.97 (0.79)	0.98 (0.89)
$\mathcal{A}$	7.3	128.6	53.3	19.8	50.0
$t_f$	2.0	35	9.4	3.0	13

STIRAP deteriorates when increasing  $\delta$  [92,93]. Furthermore, the optimization for the other sequences with  $\delta \neq 0$  is nontrivial, and there is not much literature about it—to our best knowledge. To compare the robustness of the earlier discovered pulse sequences, we also report in Table I the population transfer in the presence of two-photon detuning  $\delta/2\pi = 0.2$ . We stress that no training or further optimizations have been made to account for the new  $\delta$ . Therefore, based on Table I, we conclude that (i) PINNs can reach high fidelities in a short time under low energy consumption and (ii) PINNs are very robust when initial training parameters are changed, delivering better results in comparison with standard methods. In [68], we show that PINNs can be easily trained to counteract the adversary effect of  $\delta$ .

Finally, we extend our calculations to a four-level system and show that our PINN performs well against crosstalk to the newly added state, and also we check that our protocol deals with larger systems [68].

In this Letter, we introduced a physics-informed neural network to find control functions in open quantum systems. We demonstrated a data-free deep learning approach that jointly solves the open dynamics of quantum systems and the inverse design of control functions. First, we applied this formalism to prepare a Gibbs state in a two-level system. Second, we applied it to state-to-state transfer in a three-level system. We found that the PINN provides a flexible method that adapts to different parameters, initial states, noise channels, and power consumption requirements. We hope that PINNs will be very attractive for problems such as adiabatic quantum computing, quantum gates, state preservation, manipulation in high-dimensional Hilbert spaces, initialization of entangled states, and time-dependent induced behavior in many-body systems.

A. N. and R. C acknowledge the financial support from the projects Fondecyt Iniciación No. 11220266 and No. 11180143, respectively. F. J. G. acknowledges support from Universidad Mayor through the Doctoral fellowship.

\* ariel.norambuena@umayor.cl

† raul.coto@protonmail.com

- [1] P. Jamonneau, G. Hétet, A. Dréau, J.-F. Roch, and V. Jacques, *Phys. Rev. Lett.* **116**, 043603 (2016).
- [2] Y. Lin, J. Gaebler, F. Reiter, T. R. Tan, R. Bowler, A. S. Sørensen, D. Leibfried, and D. J. Wineland, *Nature (London)* **504**, 415 (2013).
- [3] A. M. Brańczyk, P. E. M. F. Mendonca, A. Gilchrist, A. C. Doherty, and S. D. Bartlett, *Phys. Rev. A* **75**, 012329 (2007).
- [4] M. S. Blok, C. Bonato, M. L. Markham, D. J. Twitchen, V. V. Dobrovitski, and R. Hanson, *Nat. Phys.* **10**, 189 (2014).
- [5] V. Montenegro, R. Coto, V. Ereameev, and M. Orszag, *Phys. Rev. A* **96**, 053851 (2017).
- [6] A. Bacciotti and L. Rosier, *Liapunov Functions and Stability in Control Theory*, 2nd ed. (Springer, London, 2001).

- [7] Y.-Q. Wang, Y. Wang, X. Zhao, J. Song, and Y. Xia, *Quantum Inf. Process.* **20**, 404 (2021).
- [8] J. Cui, R. van Bijnen, T. Pohl, S. Montangero, and T. Calarco, *Quantum Sci. Technol.* **2**, 035006 (2017).
- [9] F. Schäfer, M. Kloc, C. Bruder, and N. Lörch, *Mach. Learn.* **1**, 035009 (2020).
- [10] L. Coopmans, D. Luo, G. Kells, B. K. Clark, and J. Carrasquilla, *PRX Quantum* **2**, 020332 (2021).
- [11] S. Cong, *Control of Quantum Systems: Theory and Methods*, 1st ed. (Wiley, Singapore, 2014).
- [12] L. Viola, E. Knill, and S. Lloyd, *Phys. Rev. Lett.* **82**, 2417 (1999).
- [13] L. Viola and E. Knill, *Phys. Rev. Lett.* **94**, 060502 (2005).
- [14] Xing-Long Zhen, Fei-Hao Zhang, Guanru Feng, Hang Li, and Gui-Lu Long, *Phys. Rev. A* **93**, 022304 (2016).
- [15] J. Liu and S. Cong, *Proceedings of the 2011 9th IEEE International Conference on Control and Automation (ICCA)* (Institute of Electrical and Electronics Engineers (IEEE), Santiago, 2011), pp. 318–323.
- [16] S. L. Wu and W. Ma, *Phys. Rev. A* **105**, 012204 (2022).
- [17] Y.-X. Du, Z.-T. Liang, W. Huang, H. Yan, and S.-L. Zhu, *Phys. Rev. A* **90**, 023821 (2014).
- [18] M. Anderlini, P. J. Lee, B. L. Brown, J. Sebby-Strabley, W. D. Phillips, and J. V. Porto, *Nature (London)* **448**, 452 (2007).
- [19] G. Calajo, M. J. A. Schuetz, H. Pichler, M. D. Lukin, P. Schneeweiss, J. Volz, and P. Rabl, *Phys. Rev. A* **99**, 053852 (2019).
- [20] D. Tancara, A. Norambuena, R. Peña, G. Romero, F. Torres, and R. Coto, *Phys. Rev. A* **103**, 053708 (2021).
- [21] B. B. Zhou, A. Baksic, H. Ribeiro, C. G. Yale, F. J. Heremans, P. C. Jerger, A. Auer, G. Burkard, A. A. Clerk, and D. D. Awschalom, *Nat. Phys.* **13**, 330 (2017).
- [22] Jiazhao Tian, Tianyi Du, Yu Liu, Haibin Liu, Fangzhou Jin, Ressa S. Said, and Jianming Cai, *Phys. Rev. A* **100**, 012110 (2019).
- [23] D. Leibfried, R. Blatt, C. Monroe, and D. Wineland, *Rev. Mod. Phys.* **75**, 281 (2003).
- [24] C. Altafini and F. Ticozzi, *IEEE Trans. Autom. Control* **57**, 1898 (2012).
- [25] G. Carleo and M. Troyer, *Science* **355**, 602 (2017).
- [26] Z. Cai and J. Liu, *Phys. Rev. B* **97**, 035116 (2018).
- [27] K. Choo, G. Carleo, N. Regnault, and T. Neupert, *Phys. Rev. Lett.* **121**, 167204 (2018).
- [28] G. Torlai and R. G. Melko, *Phys. Rev. Lett.* **120**, 240503 (2018).
- [29] A. Nagy and V. Savona, *Phys. Rev. Lett.* **122**, 250501 (2019).
- [30] M. J. Hartmann and G. Carleo, *Phys. Rev. Lett.* **122**, 250502 (2019).
- [31] F. Vicentini, A. Biella, N. Regnault, and C. Ciuti, *Phys. Rev. Lett.* **122**, 250503 (2019).
- [32] N. Yoshioka and R. Hamazaki, *Phys. Rev. B* **99**, 214306 (2019).
- [33] J. Carrasquilla and G. Torlai, *PRX Quantum* **2**, 040201 (2021).
- [34] Rouven Koch and Jose L. Lado, *Phys. Rev. Res.* **3**, 033102 (2021).

- [35] B. Gardas, M. M. Rams, and J. Dziarmaga, *Phys. Rev. B* **98**, 184304 (2018).
- [36] Z. Liu, L.-M. Duan, and D.-L. Deng, *Phys. Rev. Res.* **4**, 013097 (2022).
- [37] M. Reh, M. Schmitt, and M. Gartner, *Phys. Rev. Lett.* **127**, 230501 (2021).
- [38] D. Luo, Z. Chen, J. Carrasquilla, and B. K. Clark, *Phys. Rev. Lett.* **128**, 090501 (2022).
- [39] P. P. Mazza, D. Zietlow, F. Carollo, S. Andergassen, G. Martius, and I. Lesanovsky, *Phys. Rev. Res.* **3**, 023084 (2021).
- [40] M. Y. Niu, S. Boixo, V. N. Smelyanskiy, and H. Neven, *npj Quantum Inf.* **5**, 33 (2019).
- [41] Tangyou Huang, Yue Ban, E. Ya. Sherman, and Xi Chen, *Phys. Rev. Appl.* **17**, 024040 (2022).
- [42] D. Castaldo, M. Rosa, and S. Corni, *Phys. Rev. A* **103**, 022613 (2021).
- [43] Thomas Fasel, Petru Tighineanu, Talitha Weiss, and Florian Marquardt, *Phys. Rev. X* **8**, 031084 (2018).
- [44] Y. X. Zeng, J. Shen, S. C. Hou, T. Gebremariam, and C. Li, *Phys. Lett. A* **384**, 126886 (2020).
- [45] J. Brown, P. Sgroi, L. Giannelli, G. S. Paraoanu, E. Paladino, G. Falci, M. Paternostro, and A. Ferraro, *New J. Phys.* **23**, 093035 (2021).
- [46] V. V. Sivak, A. Eickbusch, H. Liu, B. Royer, I. Tsioutsios, and M. H. Devoret, *Phys. Rev. X* **12**, 011059 (2022).
- [47] M. Raissi, P. Perdikaris, and G. E. Karniadakis, *J. Comput. Phys.* **378**, 686 (2019).
- [48] G. E. Karniadakis, I. G. Kevrekidis, L. Lu, P. Perdikaris, S. Wang, and L. Yang, *Nat. Rev. Phys.* **3**, 422 (2021).
- [49] J. A. Sirignano and K. Spiliopoulos, *J. Comput. Phys.* **375**, 1339 (2018).
- [50] S. Zeng, Z. Zhang, and Q. Zou, *J. Comput. Phys.* **463**, 111232 (2022).
- [51] D. Pfau, J. S. Spencer, A. G. D. G. Matthews, and W. M. C. Foulkes, *Phys. Rev. Res.* **2**, 033429 (2020).
- [52] Z. Zhu, M. Mattheakis, W. Pan, and E. Kaxiras, *Phys. Rev. Res.* **5**, 043084 (2023).
- [53] J. M. Martyn, K. Najafi, and D. Luo, *Phys. Rev. Lett.* **131**, 081601 (2023).
- [54] M. Angeli, G. Neofotistos, M. Mattheakis, and E. Kaxiras, *Chaos Solitons Fractals* **154**, 111621 (2021).
- [55] S. A. Desai, M. Mattheakis, D. Sondak, P. Protopapas, and S. J. Roberts, *Phys. Rev. E* **104**, 034312 (2021).
- [56] M. Mattheakis, D. Sondak, A. S. Dogra, and P. Protopapas, *Phys. Rev. E* **105**, 065305 (2022).
- [57] X. Fang, K. Kruse, T. Lu, and J. Wang, *Rev. Mod. Phys.* **91**, 045004 (2019).
- [58] C. Letellier, I. Sendiña-Nadal, E. Bianco-Martinez, and M. S. Baptista, *Sci. Rep.* **8**, 3785 (2018).
- [59] A. Hannachi, *Phys. Rev. E* **60**, 429 (1999).
- [60] A. Tacchella, D. Mazzilli, and L. A. Pietronero, *Nat. Phys.* **14**, 861 (2018).
- [61] S. Denisov, J. Klafter, and M. Urbakh, *Phys. Rev. E* **66**, 046203 (2002).
- [62] D. Harnack, E. Laminski, M. Schunemann, and K. R. Pawelzik, *Phys. Rev. Lett.* **119**, 098301 (2017).
- [63] U. Gungordu and J. P. Kestner, *Phys. Rev. Res.* **4**, 023155 (2022).
- [64] W. H. Fleming and R. W. Rishel, *Deterministic and Stochastic Optimal Control* (Springer-Verlag, New York, 1975).
- [65] K. Hornik, *Neural Netw.* **4**, 251 (1991).
- [66] M. Mattheakis, D. Sondak, A. S. Dogra, and P. Protopapas, *Phys. Rev. E* **105**, 065305 (2022).
- [67] A. Paszke *et al.*, PyTorch: An Imperative Style, High-Performance Deep Learning Library, 33rd Conference on Neural Information Processing Systems (NeurIPS, Vancouver, Canada, 2017).
- [68] See Supplemental Material at <http://link.aps.org/supplemental/10.1103/PhysRevLett.132.010801> for more details and applications of the proposed method based on PINNs, which includes Refs. [65,68–74].
- [69] A. Paszke, S. Gross, S. Chintala, G. Chanan, E. Yang, Z. Devito, Z. Lin, A. Desmaison, L. Antiga, and A. Lerer, Automatic differentiation in PyTorch, Conference on Neural Information Processing Systems (NeurIPS, Long Beach, California, 2017).
- [70] Z. Zhu, M. Mattheakis, W. Pan, and E. Kaxiras, *Phys. Rev. Res.* **5**, 043084 (2023).
- [71] D. Guéry-Odelin, A. Ruschhaupt, A. Kiely, E. Torrontegui, S. Martínez-Garaot, and J. G. Muga, *Rev. Mod. Phys.* **91**, 045001 (2019).
- [72] Luigi Giannelli and Ennio Arimondo, *Phys. Rev. A* **89**, 033419 (2014).
- [73] X. Chen, I. Lizuain, A. Ruschhaupt, D. Guéry-Odelin, and J. G. Muga, *Phys. Rev. Lett.* **105**, 123003 (2010).
- [74] X. Chen, E. Torrontegui, and J. G. Muga, *Phys. Rev. A* **83**, 062116 (2011).
- [75] H. Sun, N. Xu, S. Fan, and M. Liu, *Ann. Phys. (Amsterdam)* **418**, 168200 (2020).
- [76] D. P. Kingma and J. Ba, [arXiv:1412.6980v9](https://arxiv.org/abs/1412.6980v9).
- [77] R. Sagastizabal, S. P. Premaratne, B. A. Klaver *et al.*, *npj Quantum Inf.* **7**, 130 (2021).
- [78] D. Ran, Wu-Jiang Shan, Zhi-Cheng Shi, Zhen-Biao Yang, J. Song, and Y. Xia, *Phys. Rev. A* **101**, 023822 (2020).
- [79] W. Wu and Ze-Zhou Zhang, *Sci. Rep.* **11**, 7188 (2021).
- [80] K.-J. Boller, A. Imamoglu, and S. E. Harris, *Phys. Rev. Lett.* **66**, 2593 (1991).
- [81] M. Fleischhauer, A. Imamoglu, and J. P. Marangos, *Rev. Mod. Phys.* **77**, 633 (2005).
- [82] E. Arimondo and G. Orriols, *Lett. Nuovo Cimento* **17**, 333 (1976).
- [83] I. V. Jyotsna and G. S. Agarwal, *Phys. Rev. A* **52**, 3147 (1995).
- [84] J. R. Kuklinski, U. Gaubatz, F. T. Hioe, and K. Bergmann, *Phys. Rev. A* **40**, 6741 (1989).
- [85] K. Bergmann, H. Theuer, and B. W. Shore, *Rev. Mod. Phys.* **70**, 1003 (1998).
- [86] F. J. González and R. Coto, *Quantum Sci. Technol.* **7**, 025015 (2022).
- [87] R. Coto, V. Jacques, G. Hétet, and J. R. Maze, *Phys. Rev. B* **96**, 085420 (2017).
- [88] X. Laforgue, G. Dridi, and S. Guerin, *Phys. Rev. A* **105**, 032807 (2022).
- [89] X. Chen and J. G. Muga, *Phys. Rev. A* **86**, 033405 (2012).

- [90] Y.-Z. Lai, J.-Q. Liang, H. J. W. Müller-Kirsten, and J.-G. Zhou, *Phys. Rev. A* **53**, 3691 (1996).
- [91] A. Baksic, H. Ribeiro, and A. A. Clerk, *Phys. Rev. Lett.* **116**, 230503 (2016).
- [92] V. I. Romanenko and L. P. Yatsenko, *Opt. Commun.* **140**, 231 (1997).
- [93] N. V. Vitanov, A. A. Rangelov, B. W. Shore, and K. Bergmann, *Rev. Mod. Phys.* **89**, 015006 (2017).